

High-resolution surface photometry of the core of NGC 4151

Roberto Terlevich,¹ Miguel Sánchez Portal,² Angeles I. Díaz² and Elena Terlevich¹

¹Royal Greenwich Observatory, Madingley Road, Cambridge CB3 0EZ

²Departamento de Física Teórica, C-XI, Universidad Autónoma de Madrid, Cantoblanco, 28049-Madrid, Spain

Accepted 1990 October 2. Received 1990 September 24; in original form 1990 April 23

SUMMARY

CCD images of the Seyfert type 1 galaxy NGC 4151 were obtained under excellent seeing conditions (FWHM ≈ 0.7 arcsec). The images were taken through broad-band V , R and I , and narrow-band $H\alpha$ filters. Analysis of the data shows a complex structure in a region of about 4 arcsec around the nucleus. We found two main systems: (i) an elongated structure present in V , R and narrow $H\alpha$ at PA $\approx 60^\circ$, extended over ≈ 4 arcsec. The colour maps corresponding to the inner 2-arcsec region of this structure show two unresolved components situated each side of the nucleus at PA $\approx 75^\circ$ which appear to be spatially coincident with both the arcsec scale radio-jets and the narrow emission line region; and (ii) a nuclear ‘bar’ of ≈ 1 -arcsec length, seen only on the R frame, at PA $= 150^\circ$. This ‘bar’ may be caused by anisotropies in the NLR distribution. Alternatively, it may represent an extended BLR which might be due either to scattering of nuclear light by a toroid that also collimates the nuclear radio jets or can be a truly extended BLR, a consequence of sporadic supernova outbursts.

1 INTRODUCTION

NGC 4151, classified as an Sab galaxy (Sandage & Tammann 1981), is the closest and best studied of the bright Seyfert 1 galaxies. The optical structure of its nucleus consists of a point-like component usually associated with the broad-line region (BLR) and known to vary in time-scales of a few weeks to a few years (Lyutyi & Oknyanskii 1987; Gill *et al.* 1984). The narrow-line region (NLR) extends over less than 4 arcsec at PA $\approx 60^\circ$ (e.g. Ulrich 1973), and the extended narrow-line region (ENLR) covers about 15 arcsec to the south-west and about 5 arcsec to the north-east at PA $\approx 50^\circ$ (Penston *et al.* 1990; Pérez *et al.* 1989). All this structure is embedded in a bulge of about 3×2 arcmin.

Although in many other Seyfert galaxies the NLR is more extended along the general direction of the radio axis, in the case of NGC 4151 the agreement is not good. The radio-structure is a collection of resolved sources (at 1 pc scale), where the collimation direction is not conserved. The nuclear jets at arcsec scale are oriented at PA $\sim 70^\circ$ – 80° and misaligned with the ENLR by $\sim 30^\circ$ (Johnston *et al.* 1982; Booler, Pedlar & Davies 1982; Harrison *et al.* 1986). At the smaller scales, the radio component that might be associated with the nucleus, is elongated at PA $= 57^\circ$ similar to the PA of the most extended optical features of the ENLR (Heckman & Balick 1986; Harrison *et al.* 1986). This fact has led Harrison *et al.* (1986) to hypothesize that the ultraviolet (UV) responsible for the ionization of the ENLR is in fact collimated at the smaller scales.

Recent interest on the role played by anisotropy in the radiation field close to the nucleus has prompted studies of the inner structure of some nearby Seyfert galaxies (Tadhunter & Tsvetanov 1989). In a recent paper based on narrow-band CCD imaging in the [O III] $\lambda 5007$ Å and $H\alpha$ lines, Pérez *et al.* (1989) reported a low [O III]/ $H\alpha$ ratio central band of ≈ 1 -arcsec length at PA $= 133^\circ$ across the nucleus in addition to the already known structures. Pérez *et al.* concluded that this band represents a central region of low ionization or high reddening (torus or disc) also responsible for the anisotropy of the radiation field. The same structure is present in the [O III] $\lambda 5007$ Å and $H\alpha$ maps of Pérez-Fournon & Wilson (1990).

Challenging the canonical picture of active galactic nuclei, Terlevich and collaborators (Terlevich & Melnick 1985; Terlevich, Melnick & Moles 1987; Terlevich 1989b) have suggested that at least *some* of the objects classified as Seyfert galaxies can be understood in terms of nuclear star formation. The high ionization inferred from the observed emission line spectra can be the consequence of a preferred formation of very hot massive Wolf–Rayet stars in the metal-rich nuclear regions, and the broad permitted emission lines and their variability can be due to supernova activity (Terlevich & Melnick 1985, 1988; Terlevich 1989b; Filippenko 1989). The interaction of stellar winds and supernova ejecta from the starburst with the ambient nuclear interstellar matter can be shown to generate a kiloparsec (kpc) scale collimated ejecta perpendicular to the nuclear principal plane (Tomisaka & Ikeuchi 1988).

One fundamental difference between the starburst scenario and the traditional one of a black hole surrounded by an accretion disc, is the predicted extent of the BLR. In the black hole scenario the BLR is a single compact object less than a parsec (pc) across. In the starburst scenario the BLR is produced, instead, by a population of supernovae and supernova remnants spread over the nuclear star-forming region. Terlevich (1989a,b) estimated that the size of this star-forming region for a galaxy with nuclear luminosity like that of NGC 4151, will be between 0.2 and 1 arcsec FWHM and predicted that some nearby Seyfert type 1 galaxies should show a resolved BLR if more than one bright supernova remnant is observed simultaneously.

The only reported observation of an upper limit on the size of the core of NGC 4151 below 0.2 arcsec is that of Schwarzschild (1973). Based on the Stratoscope observations he gives an upper limit of 0.08 arcsec for the nuclear component. Analysis of the light curve before and after the flight (Lloyd 1984) indicates that, at the time of the observation, the nucleus of NGC 4151 was very bright and near a maximum. The amplitude and shape of the light curve, from a few weeks before to about two years after, is compatible with the theoretical expectations for the light curve of a supernova and supernova remnant evolving in a high density environment (Terlevich, in preparation). Therefore, Schwarzschild's failure to resolve the nuclear region of NGC 4151, could be the consequence of the nuclear light being dominated by a single recent supernova event.

In order to search for structure at sub-arcsec scale, we started a CCD imaging survey of nearby AGNs at La Palma where the seeing is usually excellent. Here we report the first imaging results in NGC 4151.

2 OBSERVATIONS AND DATA REDUCTION

Our observations of NGC 4151 were made in 1988 May 6/7 with a blue sensitive GEC CCD at the $f/15$ Cassegrain focus of the 1.0-m Jacobus Kapteyn Telescope (JKT) of the Isaac Newton Group at the Observatorio del Roque de los Muchachos, La Palma. The scale obtained with this instrumental configuration is 0.30 arcsec pixel⁻¹. Broad-band V , R and I (Kitt Peak National Observatory) and narrow-band $H\alpha$ interference filters were used. Their characteristics are summarized in Table 1. Conditions were photometric during the observations, and the seeing was excellent (a mean of 0.80 arcsec FWHM). Two images were taken of the object in each filter, with exposure times between 50 and 500 s. In practice, the images obtained during the best seeing period (0.7 arcsec FWHM) were chosen for this study.

Two stars were included in the galaxy frames, one of them very close to the edge of the chip. For the other one the measured FWHM of the combined images in the different filters were: 0.79, 0.76, 0.76, 0.79 for V , R , I and $H\alpha$, respectively.

Table 1. Filter characteristics.

Filter	λ_0 (Å)	FWHM (Å)	τ_{\max} (%)
V	5470	938	80
R	6455	1253	87
I	8300	1813	85
$H\alpha$ ($z=0$)	6563	53	50

The data reduction was carried out using the ASPIC and FIGARO software routines, as implemented on the VAX 11/780 STARLINK node at the Royal Greenwich Observatory, plus a private package kindly provided by Robert Jedrzejewski. The first reduction consisted of subtraction of the bias dark current level of the chip and division by a normalized flat field. The bias frame for each image was constructed by adding its mean bias level from the overscan columns, to a 'mean bias noise frame'. This latter frame is the average of all the bias frames taken during the night minus its mean value, and smoothed with a top-hat function. The flat-field frame was obtained by averaging a number of flat fields taken throughout the observing run. This average was then bias-subtracted and normalized to 1. Sky subtraction was performed by averaging the mean count value in several boxes in the periphery of the frame outside the bulge of the galaxy. The images were then transformed from count/pixel units to instrumental mag arcsec⁻² ones, and corrected for atmospheric and galactic extinction. The estimated galactic extinction (Burstein & Heiles 1984) is $E(B-V)=0.00$ and the intrinsic reddening derived from UV observations (Penston *et al.* 1981) is $E(B-V)=0.05$ which has been the value finally chosen to correct our images.

The V , R and I frames were calibrated using photometric standard stars from Landolt (1983). The $H\alpha$ image was calibrated using spectrophotometric standards (Stone 1977; Massey *et al.* 1988); aperture photometry was performed over the standard star frames, and the obtained CCD instrumental magnitudes (corrected for atmospheric extinction) were plotted against the published photoelectric magnitudes and fitted by the simple linear regression lines:

$$V = 0.984 V_0 + 21.635 \quad (\text{rms} = 0.010);$$

$$R = 0.998 R_0 + 21.947 \quad (\text{rms} = 0.038);$$

$$I = 0.993 I_0 + 21.106 \quad (\text{rms} = 0.022);$$

$$M(H\alpha) = 1.070 M_0(H\alpha) + 35.327 \quad (\text{rms} = 0.030).$$

The above calibrations are homogeneous and internally consistent but, since our broad-band filter set is not standard, care should be taken when comparing our data with other observations.

To produce the $H\alpha$ emission image, the continuum adjacent to the line has to be eliminated. This has been done by considering the line and continuum contributions to each of the $H\alpha$ and R filters to the total intensities $I(H\alpha)$ and $I(R)$, i.e.,

$$I(H\alpha) = I_l \tau_{H\alpha} + I_c \int_{\Delta H\alpha} \tau_{H\alpha}(\lambda) d\lambda = I_l \tau_{H\alpha} + I_c k_{H\alpha},$$

$$I(R) = I_l \tau_R + I_c \int_{\Delta R} \tau_R(\lambda) d\lambda = I_l \tau_R + I_c k_R,$$

where $I(H\alpha)$ and $I(R)$ are the observed intensities (in counts s⁻¹) in the $H\alpha$ and R filters, respectively; $\Delta H\alpha$ and ΔR are the $H\alpha$ and R filter bandwidths (FWHM in Table 1), and $\tau(H\alpha)$ and $\tau(R)$ the corresponding filter transmissions at the redshifted $H\alpha$ wavelength (Argyle *et al.* 1988). The sub-indexes l and c denote the $H\alpha$ emission line and the continuum, respectively.

Assuming the intensity of the continuum to be constant through the bandwidth and the filter transmission also constant through the line, the intensity of the $H\alpha$ emission line can be obtained directly as

$$I_1 = \frac{I(H\alpha)k_R - I(R)k_{H\alpha}}{\tau(H\alpha)k_R - \tau(R)k_{H\alpha}}.$$

Prior to subtraction, the two frames were aligned according to the offsets derived from the centroids of a bidimensional Gaussian fit to the galactic nuclear light distribution. Subsequent comparisons with alignments performed using offsets derived from similar fittings to field star images show the accuracy of our method to be better than 0.2 pixel (0.06 arcsec).

3 RESULTS

Emission lines contribute significantly to most of the observed images. In what follows a general description of the frames is presented, while a detailed discussion of their different contributors is left for Section 4.

3.1 Broad-band and $H\alpha$ images

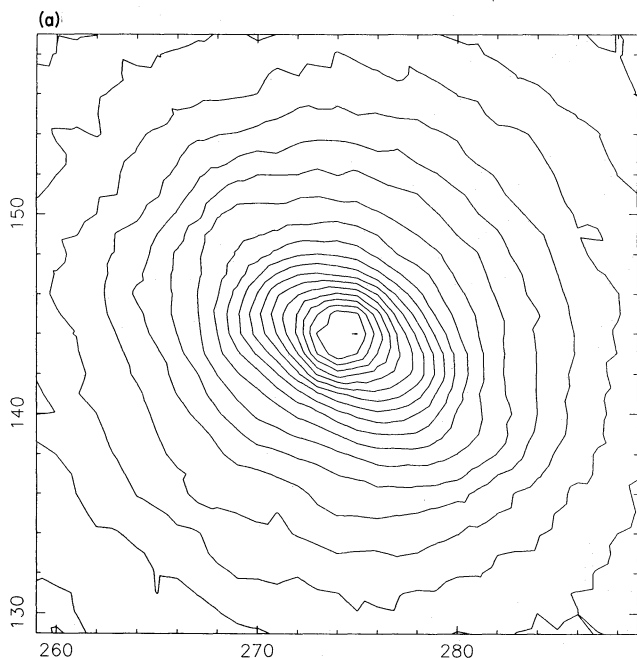
Fig. 1(a)–(c) show the isophotal maps corresponding to the three broad-band images V , R and I , respectively. Both V and R images have an elongated shape in the inner 6 arcsec. The V frame shows elliptical isophotes with major axis in the north-east–south-west direction ($PA \approx 50^\circ$) and eccentricity $1 - b/a = 0.3$. The R image shows a more complex behaviour: for the very inner zones the isophotes are elliptical ($1 - b/a$

$a = 0.2$), with major axis in the north-west–south-east direction ($PA \approx 150^\circ$), then turn circular, and finally become elliptical with eccentricity and position angle similar to the V image. The I image inner isophotal contours are almost circular; at about 6 arcsec radius they become slightly elongated with eccentricity ≈ 0.04 at $PA \approx 50^\circ$. Fig. 2 shows the isophotal map corresponding to the narrow filter $H\alpha$ image. It has an elongated structure with major axis lying in the north-east–south-west direction ($PA \approx 50^\circ$), similar to that identified in the V and R images.

3.2 Colour maps

Colour frames were constructed from the individual broad-band images, using the alignment procedure outlined in the previous section and are shown in Plate 1. In order to avoid undersampling effects, the flux calibrated images were previously smoothed with a Gaussian filter with a dispersion equal to the seeing dispersion. Fig. 3(a)–(c) show the three colour maps $V-I$, $R-I$ and $V-R$, respectively, in the inner 31 by 31 pixel (9.3 by 9.3 arcsec) of the galaxy. Inspection of these figures reveals two completely different types of behaviour for the nuclear region. Both the $V-I$ and $R-I$ colours show elliptical isophotes, with the $R-I$ somewhat rounder than the $V-I$ image, and a strong colour gradient with the circum-nuclear region being bluer than the bulge. While the $V-I$ image shows two blue blobs symmetrically located across the nucleus ($PA \approx 70^\circ$), the $R-I$ image has a slight elongation towards the south-east on top of the more general elongation at $PA \approx 60^\circ$. The $V-R$ colour, on the other hand, shows a wealth of structure. There are two blue regions lying at both sides of the nucleus in the direction of the elongation of the V and R images ($PA \approx 70^\circ$) and a red bar-like feature in the

NGC 4151 V min=18.78 max=13.78 step=0.25



NGC 4151 R min=18.48 max=12.77 step=0.23

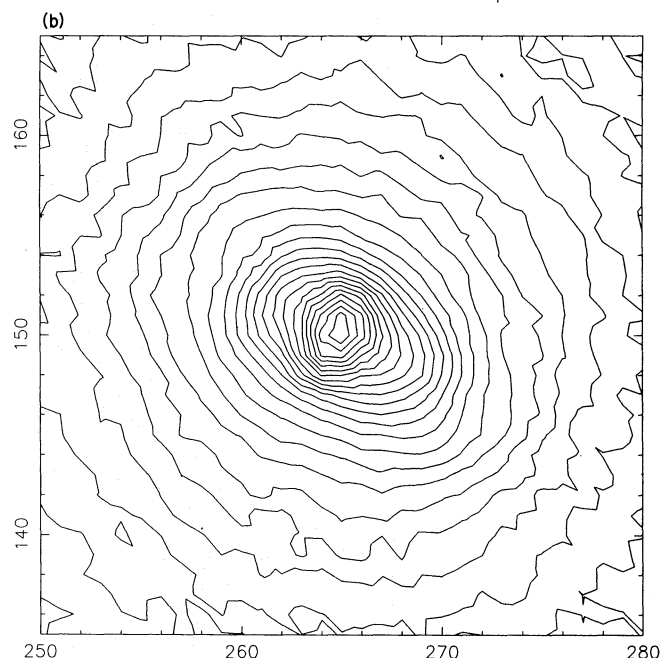


Figure 1. Isophotal maps of the nuclear region of NGC 4151; in these and following maps, north is to the top, east to the left and the scale is $0.3 \text{ arcsec pixel}^{-1}$. (a) V frame: the interval between isophotes is 0.25 mag and the maximum corresponds to $m_v = 13.8$. (b) R frame: the interval between isophotes is 0.23 mag and the maximum corresponds to $m = 12.8$. (c) I frame: the interval between isophotes is 0.25 mag and the maximum corresponds to $m = 13.1$.

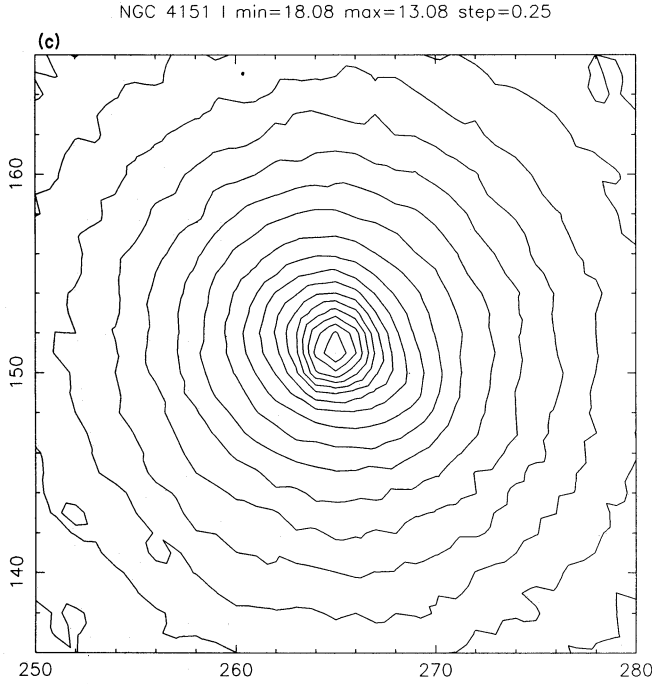


Figure 1 – continued

NGC 4151 H alpha

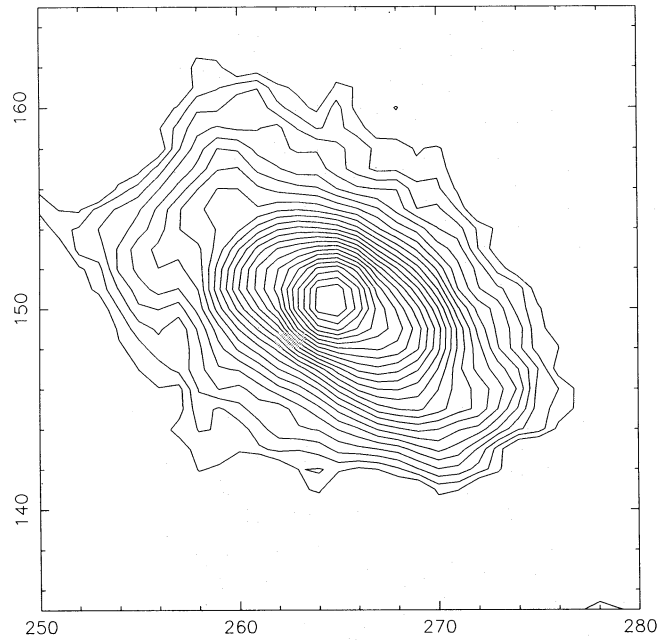


Figure 2. Isophotal map of the H α frame of the nuclear region of NGC 4151. The interval between isophotes is 0.28 mag.

direction almost perpendicular to that. It is important to note the high sensitivity of the $R-I$ colours to the H α intensity distribution. This contamination will be discussed in detail in the next section.

From the cuts of the colour frames along PA 150° (Fig. 4) we can see that, outside a region of about 6 pixel in radius (2 arcsec) the colours are consistent with those of an old stellar

population with $V-I \approx 1.1$ and $R-I \approx 0.7$ (see Pickles & Visvanathan 1985); inside the 6 pixel radius, however, the colours are substantially bluer, with $V-I$ reaching 0.4 and $R-I$ reaching -0.5 . Along PA 60° colours start to get bluer at about 4 arcsec from the nucleus. The nucleus shows up slightly redder than the circumnuclear region in the $V-I$ profile. This change in the colours of the central region is probably due to contamination by the nuclear emission lines and the nuclear blue continuum.

4 DISCUSSION

To interpret the different behaviour of the surface brightness distribution in the three broad-band images and the narrow H α one, it is first necessary to analyse the different spectral components included in the pass-band of each filter.

The V filter includes two strong emission lines: [O III] $\lambda\lambda 4959$ and 5007 \AA and some contribution of H β (broad and narrow components) at $\lambda 4861 \text{ \AA}$. The R filter includes the strong broad and narrow H α lines at $\lambda 6563 \text{ \AA}$, apart from other low-excitation forbidden lines (e.g. [O I] $\lambda\lambda 6300$, 6364 \AA , [N II] $\lambda\lambda 6548$, 6584 \AA , [S II] $\lambda\lambda 6717$, 6731 \AA). On the other hand, the I image has little contribution from strong emission lines; only the [S III] $\lambda 9069 \text{ \AA}$ line partially enters the filter where the transmission is only one fifth of the peak value.

Thus, the sources of contamination of the broad-band images are the ENLR, the NLR and the BLR present in different proportions in the V and R frames. The V filter is contaminated mainly by narrow forbidden lines and therefore maps the narrow-line region while the main contamination agent in the R filter is H α emission, both broad and narrow, with some contribution from low-excitation forbidden lines (see Fig. 5). The I filter, in contrast, is virtually free of contamination.

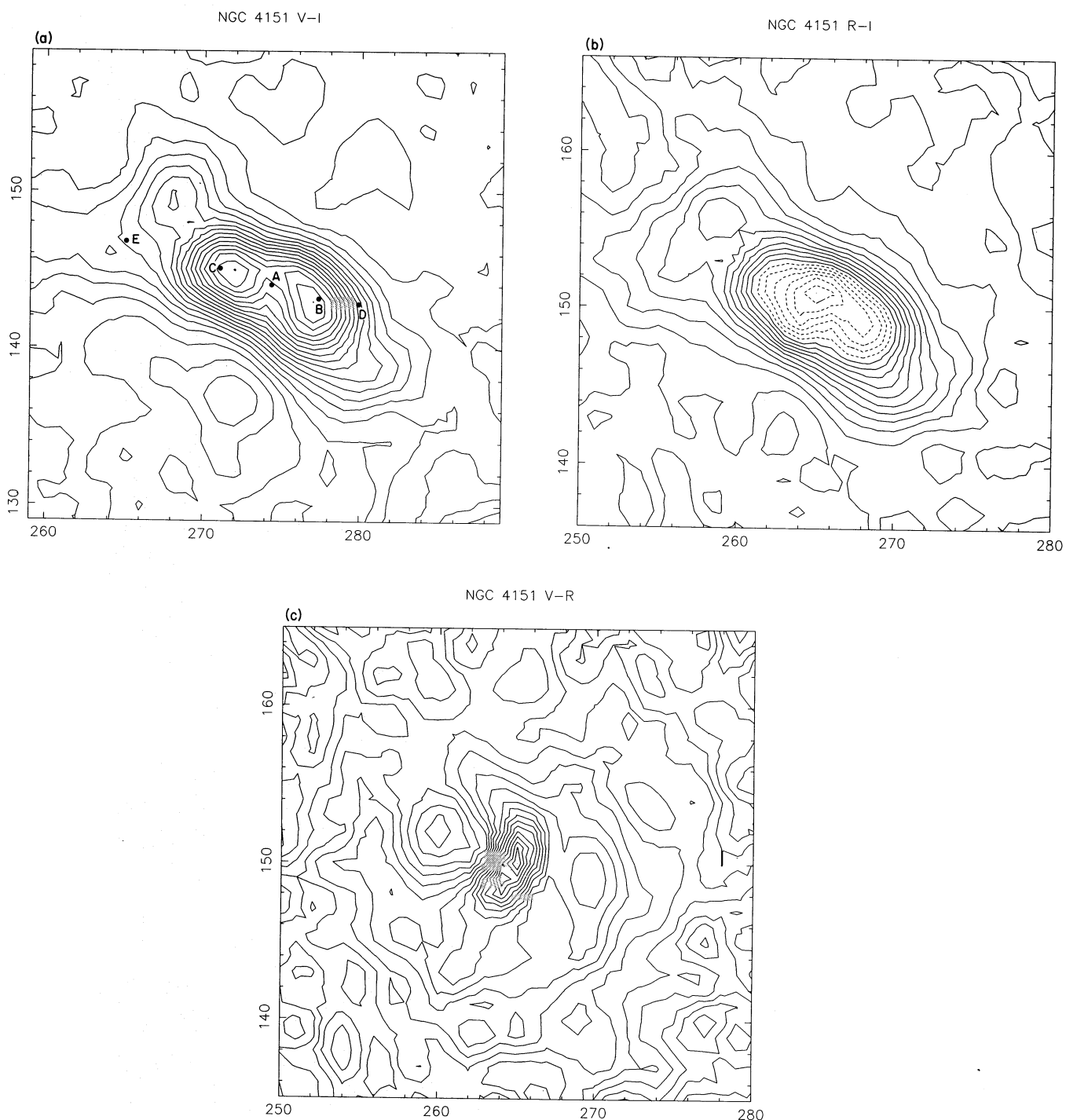


Figure 3. Colour maps of the nuclear region of NGC 4151. (a) *V-I*: the central region is bluer than the surrounding galaxy with the two minima at $PA \sim 70^\circ$ being the bluest. Positions of the radio components from Johnston *et al.* (1982), are also marked in the figure; the strongest of them (A, B and C) coincide with the nucleus and the two bluest regions, respectively. (b) *R-I*: the central region is bluer than the surrounding region, with the nucleus being the bluest. (c) *V-R*: the central region is complex in this case. A nuclear bar, redder than the surroundings, is seen along $PA \sim 150^\circ$ and two bluer regions are seen at $PA \sim 70^\circ$. These features can be better distinguished in Plate 1.

From the comparison of the *V*, *R* and *I* images (Fig. 1) we can see that, while the *I* frame shows nearly circular isophotes in the circumnuclear region, the *V* and *R* frames are elongated along $PA \approx 50^\circ$ up to about 4 arcsec from the nucleus. We can argue that the overall elongated shape of the inner parts of the *V* and *R* images probably reflects the

spatial extension of the NLR through the contribution of the different emission lines to the corresponding filters. In fact, the central structure of the *V* image is remarkably similar to that of the $[O III] \lambda\lambda 5007 \text{ \AA}$ image presented by Ebstein, Carleton & Papaliolios (1989). This interpretation is supported by the fact that the *I* frame, mainly reflecting the

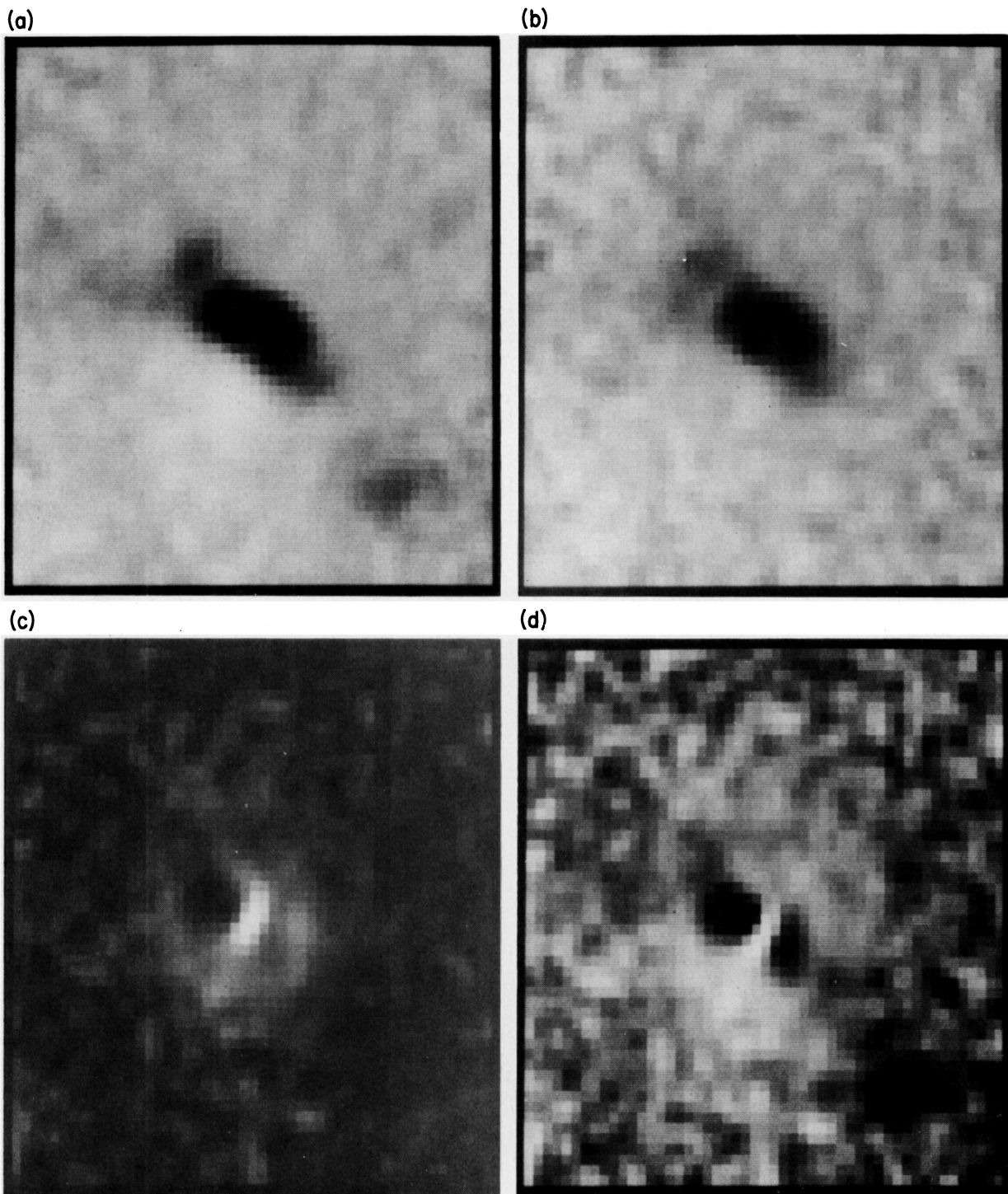


Plate 1. Colour images of the nuclear region of NGC 4151 where dark represents blue and bright, red. The scale and orientation are as described for Fig. 1. Panel (a) $V-I$, (b) $R-I$, (c) $V-R$ and (d) $V-R_c$.

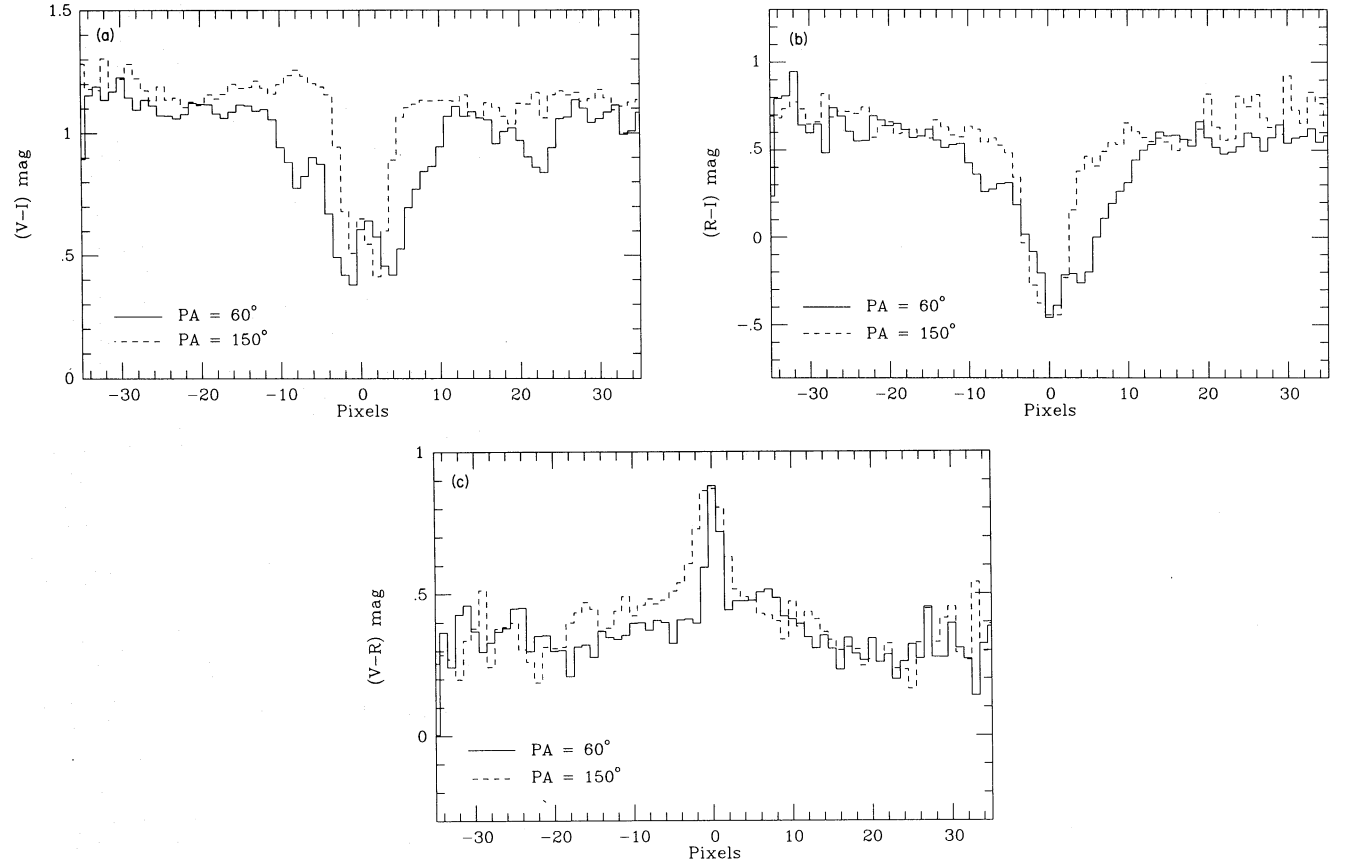


Figure 4. Colour profiles along PA 60° and 150° for (a) $V-I$, (b) $R-I$ and (c) $V-R$.

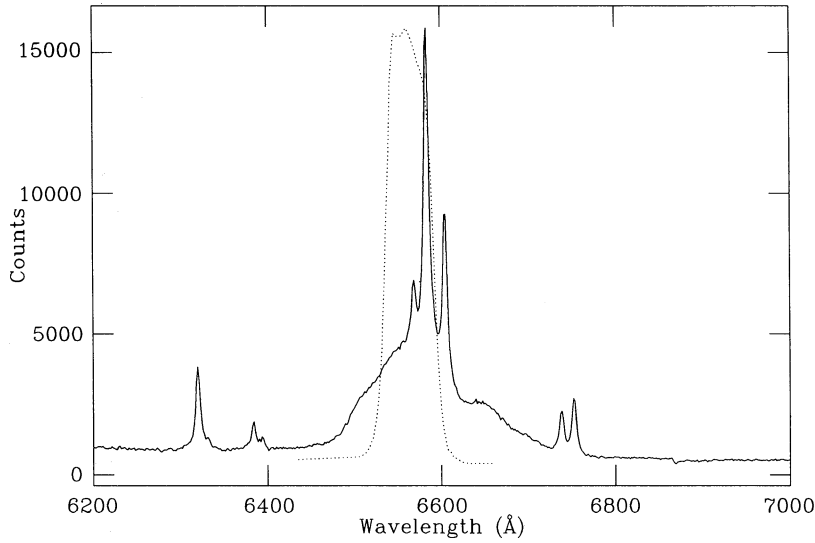


Figure 5. $H\alpha$ interference filter response curve (dotted line) superposed on to a nuclear spectrum of NGC 4151 obtained by us at the INT in January 1990. Practically all of the narrow $H\alpha$ and the core of the broad $H\alpha$ components, as well as the $[N\text{ II}]$ $\lambda 6548$ Å line, fall in the filter; not so the $[N\text{ II}]$ $\lambda 6584$ Å one.

distribution of the bulge stellar population, shows almost circular isophotes.

The $V-I$ colour image provides some information about the different distributions of $[O\text{ III}]$ and continuum light. The two central blue components observed in the frame have

positions similar to those of Ulrich's (1973) unresolved $[O\text{ III}]$ clouds II and IV. We can also compare our data with those of Ebstein *et al.* (1989). Their final speckle $[O\text{ III}]$ image, which also includes continuum light, shows an unresolved region and an extended one with a bipolar structure of about 1

arcsec in length. The continuum image shows basically the unresolved component, therefore the ratio of these two images would show a structure very similar to our $V-I$ frame. The continuum free [O III] image of Pérez *et al.* (1989) shows no unresolved component. Even the innermost isophote is elongated along the general orientation of the NLR.

In Fig. 3(a) we have also plotted the brightest radio components from the VLA map of Johnston *et al.* (1982). These data have a spatial resolution of about 0.6 arcsec, comparable to the resolution of our maps. The correlation between the optical features and the brightest radio components (A, B, C) is remarkable; the same agreement between radio and optical structure is seen in the $R-I$ and $V-R$ frames (Fig. 3b and c). Also the extent of the radio emission is similar to the central region with non-bulge colours. Therefore the colour maps seem to follow the radio distribution better than the [O III] flux distribution alone and might be showing up the NLR emission associated with the radio emission (Whittle *et al.* 1988).

In addition to the NLR elongation, the R frame shows an inner ‘bar’ perpendicular to the main elongation direction. The presence of the bar is reflected in the topology of the nuclear region in the $V-R$ colour map, which shows a striking structure in the central 4 arcsec. The red nuclear region seems to be elongated at a position angle of about 150° and a mild blue gradient is seen at $PA \approx 60^\circ$. The $R-I$ map also shows a bar, blue in this case, in the same position angle.

At small radii the $V-R$ map approximates an [O III]/ $H\alpha$ map, since line emission dominates over the continuum close to the nucleus. We can then compare our $V-R$ frame directly with the [O III]/ $H\alpha$ figure given by Pérez *et al.* (1989). The agreement between both is very good, their figure also showing the red bar where a double structure with a separation of about 0.6 arcsec can be seen.

To investigate if the origin of this behaviour can be solely the contamination by the NLR we have constructed a ‘corrected’ R frame (R_c) by subtracting from the observed one the $H\alpha$ emission frame shown in Fig. 2. The interference $H\alpha$ filter used, includes not only the narrow $H\alpha$ emission, but also [N II] $\lambda 6548 \text{ \AA}$ and part of the blue wing of the broad $H\alpha$ as illustrated in Fig. 5. This ‘corrected’ R frame is shown in Fig. 6. It can be seen that, although the external isophotes look less elongated at $PA \approx 60^\circ$ than in the uncorrected R image (Fig. 1b), the nuclear bar in the direction perpendicular to that is even more conspicuous.

The new $V-R_c$ frame (Fig. 7) also shows a clear enhancement of the structure seen in the $V-R$ image, with the mild blue gradient now becoming strong. This is a consequence of the NLR being elongated in the east-west direction. Two regions east and west of the nucleus are substantially bluer than the bulge. The nucleus itself and the extension to the south have colours that are much redder than the surrounding bulge (Fig. 8).

The new R_c-I frame (Fig. 9) also shows an enhancement of the structure seen in the $R-I$ colour frame. In particular, the bar becomes very conspicuous. These results suggest that whatever is producing the bar in the colour frames, is associated with the light distribution in the R frame. Obviously, the bar is the reflection of some peculiarities of the nuclear light distribution. But, could it be originated in a peculiar nuclear stellar distribution?

NGC 4151 R Corrected

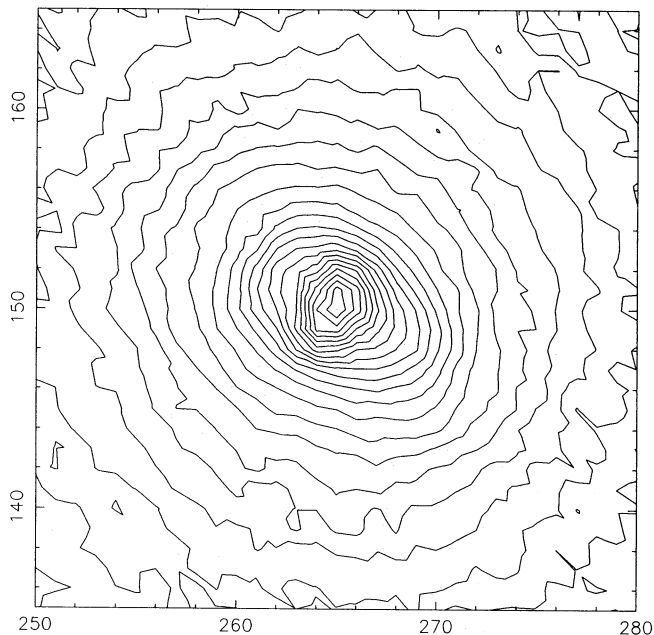
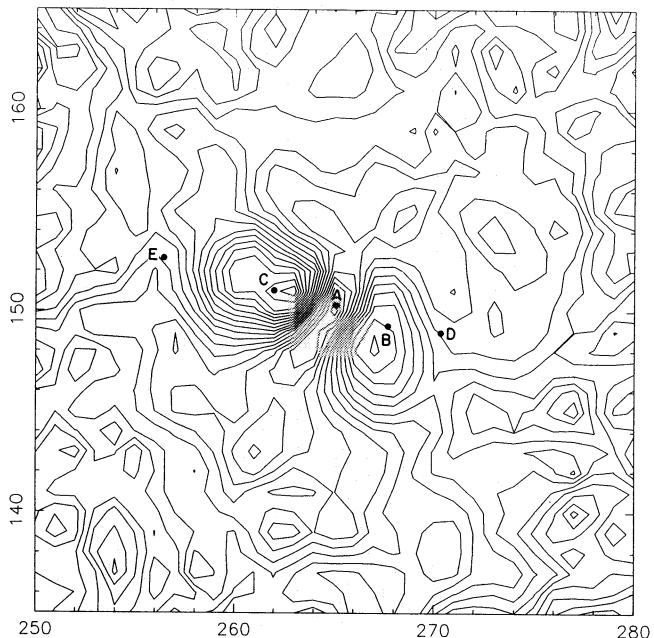
Figure 6. $H\alpha$ emission corrected R frame (R_c).

Figure 7. Corrected $V-R_c$ colour. The contrast between the red bar seen along $PA \sim 150^\circ$ and the two bluer regions at $PA \sim 70^\circ$ is larger than in the uncorrected colour (Fig. 3c). These features can be better distinguished in Plate 1. Also marked in the figure are the positions of the radio components from Johnston *et al.* (1982), the strongest of which (A, B and C) coincide with the nucleus and the two bluest regions, respectively.

The I band, as explained previously, should represent basically the bulge stellar background without much contamination from the active nucleus. In fact, from the study of the IR Ca II triplet at $\approx 8500 \text{ \AA}$ in NGC 4151, Terlevich,

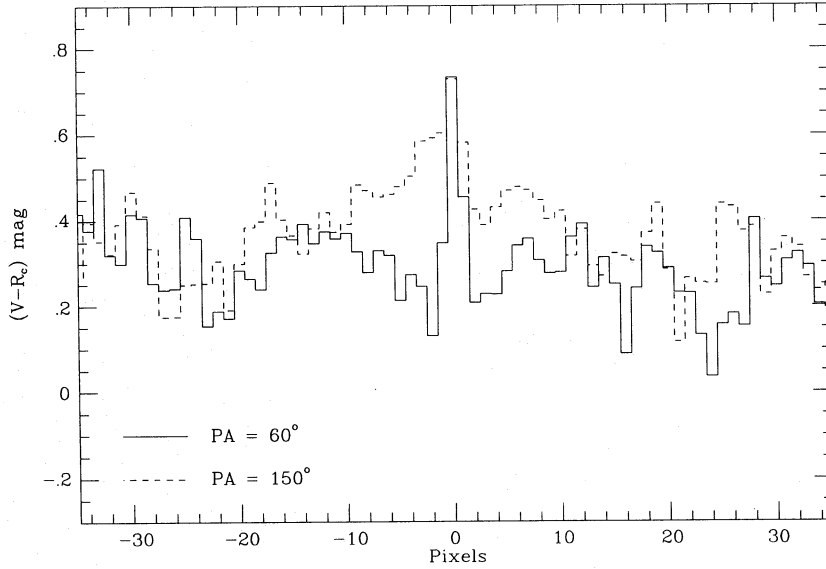


Figure 8. Corrected $V-R_c$ colour profiles at PA 60° and 150° .

NGC 4151 R_c-I

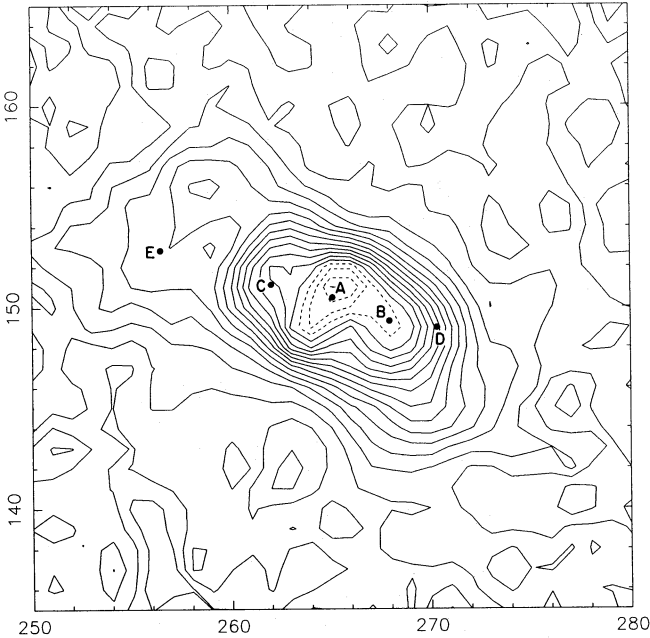


Figure 9. Corrected R_c-I colour. The red bar along PA $\sim 150^\circ$ is conspicuous. The positions of the radio components from Johnston *et al.* (1982) are also shown.

NGC 4151 Residual R

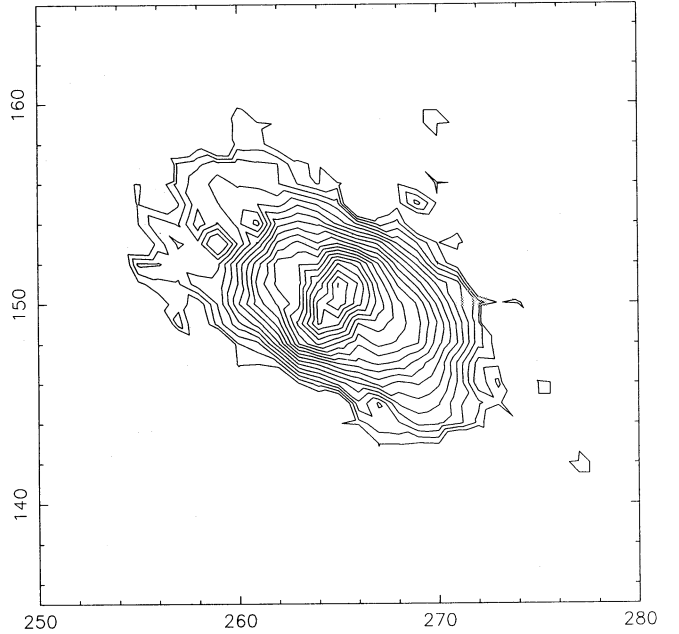


Figure 10. Residual R frame, see text for description.

Díaz & Terlevich (1990) concluded that, while the optical stellar absorption lines, like the Mg2 index at $\lambda 5172 \text{ \AA}$, are heavily diluted by the nuclear featureless continuum, the IR Ca II triplet shows only a small amount of dilution. The fact that the bar is not visible in the I band therefore, indicates that it is not a stellar feature. From the I image and using the average $R-I$ colour for an old stellar population, we constructed a 'bulge' R frame. The subtraction of this frame from the R_c one is shown in Fig. 10 and represents a detected excess of R light over that corresponding to the bulge stellar population.

However, as we mentioned above, both the narrow and the broad components of the $H\alpha$ emission, as well as [O I] $\lambda\lambda 6300, 6364 \text{ \AA}$, the [N II] strongest line and the [S II] $\lambda\lambda 6717, 6731 \text{ \AA}$ are important contaminants for the R band. Due to the width of the $H\alpha$ interference filter (53 \AA , see Table 1 and Fig. 5) and the redshift of NGC 4151, our procedure effectively eliminates the contribution of the narrow $H\alpha$ emission but neither the broad component nor the [O I], [N II] and the [S II] lines. One of those contaminating agents, or all, can be responsible for the observed emission excess. In particular, it can be seen from Fig. 5 that about two thirds of the broad component of $H\alpha$ lies outside the inter-

ference filter but inside the R filter. The resulting frame shown in Fig. 10 may contain broad and narrow emission line components.

A possibility is that the excess is due to $[\text{O I}] + [\text{N II}] + [\text{S II}]$ emission. That would require an enhanced $[\text{O I}] + [\text{N II}] + [\text{S II}]/\text{H}\alpha$ ratio in the bar with respect to the perpendicular position producing an extra component in the R filter that is not present in the $\text{H}\alpha$ one. This possibility is consistent with the data of Pérez *et al.* (1989) in which the $[\text{O III}]/\text{H}\alpha$ ratio looks generally high in the regions associated with the ENLR and very low in the bar. The fact that their low $[\text{O III}]/\text{H}\alpha$ ratio region and our R image elongation have similar sizes and orientation suggests that what is causing the excess in the R light is also causing the low $[\text{O III}]/\text{H}\alpha$ ratio. They also noted that the bar should have an artificially low value of $[\text{O III}]/\text{H}\alpha$ in the nucleus due to contamination by broad $\text{H}\alpha$ emission. However, on the implicit hypothesis of the BLR being unresolved, they concluded that the extended low $[\text{O III}]/\text{H}\alpha$ ratio was likely to be due to a low-excitation region or high reddening reducing the $[\text{O III}]$ intensity. The fact that the bar is seen in the $R-I$ frame rules out this last alternative.

The possibility of the bar representing an extended broad $\text{H}\alpha$ emission should be taken into account. NGC 4388 and Mk110 show also extended BLR perhaps associated with scattering of the nuclear source by electrons or dust (Shields & Filippenko 1988; Hutchings & Craven 1988; Hutchings & Crampton 1989). For NGC 4151 the bar could also be the signature of scattering in a torus of about 1 arcsec diameter at $\text{PA} \approx 150^\circ$. This torus may also be responsible for the collimation of the UV radiation into the ENLR (Pérez *et al.* 1989; Penston *et al.* 1990). In this case, the observed distribution of broad $\text{H}\alpha$ depends both on the distribution of emitted flux by the central source and on the distribution of scatterers. If the scatterers are in a torus oriented at $\text{PA} \approx 150^\circ$ and the illumination of the central source is roughly isotropic, we expect scattered light to come from that PA and, if the optical depth of scatterers is large, the radiation at large distances from the torus will appear to be beamed in the direction of the poles of the torus. Assuming the scatter is produced by dust particles, then a substantial amount of reddening of the underlying stellar continuum should be detected and, since not only the emission lines but also the blue featureless continuum will be scattered, we expect a very strong blue featureless continuum combined with a weak stellar contribution. Whatever the scatterers are, the blue continuum in the $\text{PA} \approx 150^\circ$ extension should be polarized.

The polarization observations of Schmidt & Miller (1980) made with a circular aperture of 2.8 arcsec diameter, are not conclusive. It was found that while the NLR is slightly polarized, 0.4 per cent at $\text{PA} = 46^\circ$, the BLR shows no polarization. The continuum was found to be polarized, at the level of 1.2–2.5 per cent, smoothly changing across the spectrum and with the polarization angle remaining constant at about $\text{PA} = 88^\circ$. The lack of polarization of the BLR argues against the scattering hypothesis for the extended BLR.

A third possibility is that we have detected a *truly extended* BLR. This possibility has been predicted by Terlevich (1989b) in the starburst scenario, where the BLR is associated with SNe and SN remnants evolving in a high-

density environment. The BLR is therefore the sum over all SNe and SN remnants that are emitting light.

The size of the BLR is determined by the spatial distribution of the remnants which, in turn, follows that of the young stars. For small SN rates, the size of the BLR is given by the dimension of a single remnant while for very high rates the characteristic size of the BLR is the core radius of the young stellar population. In the case where only a few remnants are visible at any given time, the size of the BLR has only a probabilistic meaning and the relevant parameter is the half light radius: R_{eff} (i.e. the radius containing half of the SNRs).

The size of a young cluster may be estimated using known scaling laws. Terlevich & Melnick (1981) studied the intrinsic properties of giant bursts of star formation (giant H II regions and H II galaxies). These systems are characterized by having emission lines with $\text{FWHM} > 30 \text{ Km s}^{-1}$ indicating supersonic motions in the ionized gas. Terlevich & Melnick found that giant H II regions and H II galaxies have very similar properties and follow the empirical laws

$$\text{Luminosity} \propto \sigma^4$$

$$\text{Size} \propto \sigma^2$$

The similarity of these relations to those followed by elliptical galaxies and bulges of spiral galaxies led Terlevich & Melnick to conclude that the line broadening was probably due to motions in the gravitational field of the young stars. This result was extended by Balzano (1983) to starburst nuclei. The validity of these scaling laws was recently confirmed by Melnick *et al.* (1987).

The best known giant H II region or giant burst of star formation is 30 Dor in the LMC. Moffat *et al.* (1985) showed that the surface brightness distribution of 30 Dor is well-fitted by a modified isothermal (King) profile with core radius $R_c \approx 0.2 \text{ pc}$.

Using the ratio between the $\text{H}\alpha$ luminosities of 30 Dor and NGC 4151 (~ 200 assuming a distance of 20 Mpc to NGC 4151) and the above scaling laws, we estimate that a burst with a mass distribution similar to that of 30 Dor and with the luminosity of the nucleus of NGC 4151 will have a core radius of $R_c \approx 3 \text{ pc}$, i.e. 0.03 arcsec. The relation between the core radius and the half light radius for a modified isothermal depends on the concentration parameter and is $R_{\text{eff}} = 10 R_c$ for a concentration parameter typical of elliptical galaxies, and $R_{\text{eff}} = 3 R_c$ for a concentration parameter typical of globular clusters. Assuming an intermediate behaviour for the putative young cluster in the nucleus of NGC 4151 (i.e. $R_{\text{eff}} = 6 R_c$) gives $R_{\text{eff}} \sim 0.18 \text{ arcsec}$. The corresponding effective diameter is comparable to the extension of the red excess found in our images. Therefore, if the activity in the nucleus of NGC 4151 is attributed to giant bursts of star formation, we might be seeing the region where that star formation is taking place.

5 CONCLUSIONS

We have studied the light distribution of the central regions of the Seyfert type 1 galaxy NGC 4151 using CCD images obtained under excellent seeing conditions. The main results of our investigation are summarized below.

We have resolved a nuclear compact linear structure (about 2 arcsec length) with $V-R$ colours bluer than the

surrounding bulge. This extension lies in the north-east-south-west direction at a PA of approximately 70° and coincides with the direction and position of the radio structure observed in the centre of NGC 4151 and interpreted as radio jets (Booler *et al.* 1982). The direction of the elongation is somewhat different (20°) from that of the ENLR as observed by Pérez *et al.* (1989) and Penston *et al.* (1990).

A second and more compact structure is detected in the south-east-north-west direction at a PA of approximately 150° with $V-R$ colour redder than the surrounding bulge. This structure, visible in the original R frame, has an extension of about 1 arcsec. We conclude that the red colours are the direct result of an excess emission in the R band due to anisotropies in the NLR distribution or broad $H\alpha$ contamination.

In order to investigate the anisotropy of the NLR, high spatial resolution spectroscopy along and perpendicular to the red bar are badly needed. Two possibilities are given for the origin of the broad $H\alpha$ contamination: scattering of the BLR by a centrally located nearly edge-on torus or a truly extended broad $H\alpha$ emission. In the first case, polarized scattered light perpendicular to the plane of the torus ($PA \approx 150^\circ$) is expected. Finally it is suggested that, if the starburst scenario for activity in galactic nuclei is considered, we might be seeing the actual size of the nuclear star forming region.

We hope that this paper will bring attention to the study of the structure of the core of nearby Seyfert galaxies with high resolution. This type of study is probably a very powerful discriminant of theories of nuclear activity involving star formation. On the other hand, a confirmation that the BLR remains unique and unresolved at sub-parsec scale would represent a fundamental validation of the canonical scenario.

ACKNOWLEDGMENTS

The JKT is operated in the island of La Palma by the RGO at the Observatorio del Roque de los Muchachos of the Instituto de Astrofísica de Canarias. We would like to thank CAT for awarding observing time, and the British Council and NATO for collaborative research grants. We acknowledge fruitful discussions with Jorge Melnick, Bernard Pagel, Michael Penston, Enrique Pérez, Ismael Pérez-Fournon and Clive Tadhunter. The thorough and critical reading by Mark Whittle and his many suggestions greatly improved the contents of this paper.

REFERENCES

- Argyle, R. W., Mayer, C. J., Pike, C. D. & Jorden, P. R., 1988. *A User Guide to the JKT CCD Camera*, User Manual XVIII, Isaac Newton Group, La Palma.
- Balzano, V. A., 1983. *Astrophys. J.*, **268**, 602.
- Burstein, D. Heiles, C., 1984. *Astrophys. J. Suppl.*, **54**, 33.
- Booler, R. V., Pedlar, A. & Davies, R. D., 1982. *Mon. Not. R. astr. Soc.*, **199**, 229.
- Ebstein, S. M., Carleton, N. P. & Papaliolios, C., 1989. *Astrophys. J.*, **336**, 103.
- Filippenko, A. V., 1989. *Astr. J.*, **97**, 726.
- Gill, T. R., Lloyd, C., Penston, M. V. & Snijders, M. A. J., 1984. *Mon. Not. R. astr. Soc.*, **211**, 31.
- Heckman, T. M. & Balick, B., 1986. *Astrophys. J.*, **268**, 102.
- Harrison, B., Pedlar, A., Unger, S. W., Burgess, P., Graham, D. A. & Preuss, E., 1986. *Mon. Not. R. astr. Soc.*, **218**, 775.
- Hutchings, J. B. & Crampton, D., 1989. *Astr. J.*, **99**, 37.
- Hutchings, J. B. & Craven, S. E., 1988. *Astr. J.*, **95**, 677.
- Johnston, K. J., Elvis, M., Kjer, D. & Shen, B. S. P., 1982. *Astrophys. J.*, **262**, 61.
- Kerr, F. J., 1957. *Astr. J.*, **62**, 93.
- Landolt, A. U., 1983. *Astr. J.*, **88**, 439.
- Lloyd, C., 1984. *Mon. Not. R. astr. Soc.*, **209**, 697.
- Lyutyi, V. M. & Oknyanskii, V. L., 1987. *Soviet astr.*, **31**, 245.
- Massey, P., Strobel, K., Barnes, J. V. & Anderson, E., 1988. *Astrophys. J.*, **328**, 315.
- Melnick, J., Moles, M., Terlevich, R. & García-Pelayo, J.-M., 1987. *Mon. Not. R. astr. Soc.*, **226**, 849.
- Moffat, J. W., Seggewiss, W. & Shara, M. M., 1985. *Astrophys. J.*, **295**, 109.
- Penston, M. V. *et al.*, 1981. *Mon. Not. R. astr. Soc.*, **196**, 857.
- Penston, M. V. *et al.*, 1990. *Astr. Astrophys.*, **236**, 53.
- Pérez, E., González-Delgado, R., Tadhunter, C. & Tsvetanov, Z., 1989. *Mon. Not. R. astr. Soc.*, **241**, 31p.
- Pérez-Fournon, I. & Wilson, A. S., 1990. *Astrophys. J.*, **356**, 456.
- Pickles, A. J. & Visvanathan, N., 1985. *Astrophys. J.*, **294**, 134.
- Sandage, A. & Tammann, G. A., 1981. *Revised Shapley-Ames Catalog of Bright Galaxies*, Carnegie Institution of Washington, Washington DC.
- Schmidt, G. D. & Miller, J. S., 1980. *Astrophys. J.*, **240**, 759.
- Schwarzschild, M., 1973. *Astrophys. J.*, **182**, 357.
- Shields, J. C. & Filippenko, A. V., 1988. *Astrophys. J.*, **332**, L55.
- Stone, R. P. S., 1977. *Astrophys. J.*, **218**, 767.
- Tadhunter, C. & Tsvetanov, Z., 1989. *Nature*, **341**, 422.
- Terlevich, E., Díaz, A. I. & Terlevich, R., 1990. *Mon. Not. R. astr. Soc.*, **242**, 271.
- Terlevich, R., 1989a. In: *Evolutionary Phenomena in Galaxies*, p. 149, eds Beckman, J. E. & Pagel, B. E. J., Cambridge University Press, Cambridge.
- Terlevich, R., 1989b. In: *Structure and Dynamics of the Interstellar Medium*, p. 343, eds Tenorio-Tagle, G., Moles, M. & Melnick, J., Springer-Verlag, Berlin.
- Terlevich, R. & Melnick, J., 1981. *Mon. Not. R. astr. Soc.*, **195**, 839.
- Terlevich, R. & Melnick, J., 1985. *Mon. Not. R. astr. Soc.*, **213**, 841.
- Terlevich, R. & Melnick, J., 1988. *Nature*, **333**, 239.
- Terlevich, R., Melnick, J. & Moles, M., 1987. In: *Observational Evidence for Activity in Galaxies*, p. 499, eds Khachikyan, E. Ye., Fricke, K. J. & Melnick, J., Reidel, Dordrecht.
- Tomisaka, K. & Ikeuchi, S., 1988. *Astrophys. J.*, **330**, 695.
- Ulrich, M. H., 1973. *Astrophys. J.*, **181**, 51.
- Whittle, M., Pedlar, A., Meurs, E. J. A., Unger, S. W., Axon, D. J. & Ward, M. J., 1988. *Astrophys. J.*, **326**, 125.